SciencePG

Science Publishing Group

One-Dimensional Shape Memory Alloys Material Phenomenological Constitutive Model Based on Stress Due to Mechanical and Chemical Energy Change

Rabiu Ahmad Abubakar

Institute of Mechanical engineering Design, Mechanical Engineering Department, Zhejiang University, Hangzhou, China

Email address:

rbkiru@yahoo.com

Abstract: Shape Memory Alloy (SMA) is a material that has the ability to memorize previous shapes after deforming. That is it regains its original shape when temperature increases, converting thermal energy to mechanical energy. This property of the plastic-like deformation which subsequently recovers its original shape is referred to as Shape Memory Effects (SMEs). The history of this material began in the year 1800s. Because of their unique behavior, SMA has great industrial applications. Many constituted models of SMA behavior are formed describing SMA behavior. Most of them are based on experimental phenomenological macroscopic constitutive models consisting of variables that reveal the degree of phase transition that describes the phenomenological macroscopic behavior of SMA. These types of models are very easy and the parameters are also very easy to determine. In this research, a constitutive model is formulated based on the obserbation of experimental data, the SMA behavior is simulated using Artificial Neural Networks (ANN). The phenomenological constitutive model comprises both mechanical and chemical change. In the parameter estimation, the Back-Progation (BP) algorithm and the nonlinear optimization algorithm are used. A numerical simulation is performed, and the phenomenological constitutive model captures well the uniaxial tension and compression experimental data, therefore the constitutive model is verified.

Keywords: NiTi Shape Memory Alloy, Phenomenological Model, Artificial Neural Network

1. Introduction

Shape Memory Alloy (SMA) is a material that has the ability to memorize previous shapes after deforming [1-3]. That is it regains its original shape when temperature increases [4, 5], converting thermal energy to mechanical energy [6-8]. This property of the plastic-like deformation which subsequently recovers its original shape is referred to as Shape Memory Effects (SMEs) [9-11]. The history of this material began in the year 1800s which is discovered by William Buchler and his coworkers [12], and the NINOL was given to the material with NI stand for nickel and NOL for Nabal ordinance laboratory in which the property was discovered first [13]. A strange loud sound is produced at the cold stage, which is a different sound at the hot stage [10]. After a decade, the noble material had drawn research's attention for various industrial applications [14, 15] like oil and gas industries [16] air vehicles [17] wind farms energy systems [18] space exploration [18] surgical tools [19] and so on. Later it was concluded this noble material has a unique behavior [20] which made it different from various alloy material, and named it NITINOL referring to the first laboratory where it was first discovered. The material can recover energy up to $106J/m^3$, and the transformation temperature depends on Ni-content with an upper limit of 363 K [21].

For the application of SMA in many fields, a good understanding of its behavior in very significant [22]. Hence, a correct model is required. SMA behavior originates at the microscopic level in the crystal lattice, and this is related to factors like temperature, stress, and loading history. There are many difficulties in coupling these factors, to accurately describe the SMA formation. Many SMA models have been proposed and established. Example of these are Falk [23]

developed a single crystal constitutive model based on Laudau theory and used Helmiltz free energy function; Abeyaratne and Knowles [24] developed a one-dimensional based on a mechanical model of Erieksen stress-induced solid-solid phase transition. Also based on macro consideration other important constitutive models are proposed. These are developed based on experimental data and internal variables that account for the degree of phase transition to show the materials macroscopic behavior. These models are very simple, and the method of parameter identification is also easy. One of these is: Tanaka et. *al* [25] proposed a classic phenomenological SMA constitutive model. And so also Liang and Rogers [26], and Brinson [27].

The research aim is to come out with a good macroscopic phenomenological constitutive model capturing both mechanical and chemical energy change in SMA structure during phase transition, and it is very significant owing to the development of entropy in SMA martensite-austenite phase transition. The main research problem and the research question involving the term accounting for chemical change in the proposed model.

2. Proposed Constitutive Model

Figure 1 shows the two lattices of the SMA of the austenite and martensite. At high temperatures, the lattice of SMA is austenite; at low temperatures, the lattice of SMA is martensite. At moderate temperatures, austenite and marten site can coexist. The phase transition results from the sliding of the lattice plane. Austenite is cubic, while marten site is tetrahedral in shape. It can be seen that the arrangement or order of atoms changes from austenite to martensite; this changes the chemical energy of the system. In Figure 1(a), all the sizes are equal, that is (a=b=c); in Figure 1(b) and (c), the sizes are not equal, that is (a, b and c are not equal).

(a) austenite (a=b=c)   (b) martensite (a, b and c are not equal)
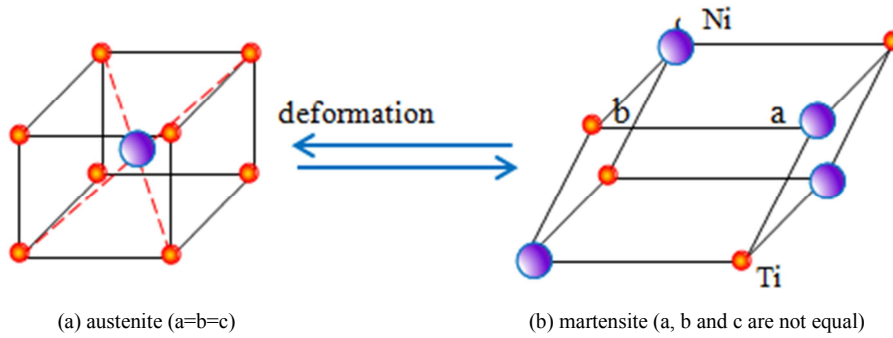
Figure 1. Schematic diagram of two SMA lattices.

The constitutive model proposed in the research is based on stress theory in ref [28] and this chemical energy change that occurs during phase transformation. When SMA material undergoes phase transformation, the free energy of the system is presented as:

$$\Theta(\varepsilon, T) = \Theta_m + \Theta_c$$

where Θ_m is the mechanical energy, and is expressed in ref. [28], Θ_c is chemical energy and is expressed as:

$$\Theta_c = -T_1 \Delta s^{A-M} \tag{1}$$

where T_1 is the reference temperature of the material, and $-\Delta s^{A-M}$ is the change in entropy, and $\Delta s^{A-M} = s_A - s_M$, with s_A as entropy at the austenite stage, s_M as entropy at the martensite stage. The negative sign accounting for the latent heat of phase transformation. When the material quantity is considered, Eq. 1 becomes:

$$\Theta_c = -\rho T_1 \Delta s^{A-M} \tag{2}$$

Eqt. 2 is further expressed in the form of stress due to chemical energy as:

$$\sigma_c = -\frac{1}{a_w l} \rho T_1 \Delta s^{A-M} \tag{3}$$

where σ_c is the stress induced by the chemical energy change, a_w is the SMA wire crossectional area, l is the total length of the SMA material, ρ is the material density.

Now the proposed model is constituted as follows:

$$\mu \frac{\partial \varepsilon}{\partial t} = \sigma_m + e(\varepsilon, T) - \frac{1}{a_w l} \rho T_1 \Delta s^{A-M}, \tag{4}$$

where $\mu \frac{\partial \varepsilon}{\partial t}$ is the viscous term, μ is a constant, σ_m is the stress induced by the mechanical energy change due to phase transformation, $e(\varepsilon, T)$ is the elastic term of stress, and is a function of strain ε and temperature T; the term $-\frac{1}{a_w l} \rho T_1 \Delta s^{A-M}$ is the chemical part due to phase transformation in the form of stress. Eq. 4 is rearranged as follows:

$$\mu \frac{\partial \varepsilon}{\partial t} = (\sigma_m - \frac{1}{a_w l} \rho T_1 \Delta s^{A-M}) + e(\varepsilon, T). \tag{5}$$

The total stress due to mechanical and chemical energy as:

$$\sigma_{total} = \sigma_m + \sigma_c = (\sigma_m - \frac{1}{a_w l}\rho T_1 \Delta s^{A-M}) \qquad (6)$$

For non-isothermal process Δs^{A-M} is computed as follows:

$$\Delta s^{A-M} = -\frac{d\sigma_m}{dT}\varepsilon_r. \qquad (7)$$

And for the isothermal process Δs^{A-M} is computed as follows:

$$\Delta s^{A-M} = -\frac{\sigma_m}{T}\varepsilon_t \qquad (8)$$

Therefore, Eq. 5 becomes:

$$\mu\frac{\partial\varepsilon}{\partial t} = [\sigma_m - \frac{1}{a_w l}\rho T_1(\frac{\sigma_m}{T}\varepsilon_t)] + e(\varepsilon, T) \qquad (9)$$

where ε_r is a transformation entropy, and its value is obtained from experimental data.

The viscous term can also be obtained from experimental data using Eq. 10, or through numerical differentiation.

$$\frac{d\varepsilon_i}{dt} = \begin{cases} \dfrac{-3\varepsilon_i + 4\varepsilon_{i+1} - \varepsilon_{i+2}}{2\Delta t}, ? & i = 0 \\[3mm] \dfrac{3\varepsilon_i - 4\varepsilon_{i-1} + \varepsilon_{i-2}}{2\Delta t} & i = n \\[3mm] \dfrac{\varepsilon_{i+1} - \varepsilon_{i-1}}{2\Delta t}, ? & else \end{cases} \qquad (10)$$

Where n is the experimental data number points, μ is obtained through linear regression.

$$\mu = (\{\dot{\varepsilon}\}^T \{\dot{\varepsilon}\}^{-1}\{\dot{\varepsilon}\}^T \{\sigma\}), \qquad (11)$$

Where $\{\}$ is the data column vector. The chemical part is obtained from the material experimental data.

Now since the term $\mu\dfrac{\partial\varepsilon}{\partial t}$ is obtained and the term $\dfrac{1}{a_w l}\rho T_1 \dfrac{\sigma_m}{T}\varepsilon_t$ can be calculated from material experimental data, the elastic term $e(\varepsilon, T)$ can be computed as:

$$e(\varepsilon, T) = \mu\frac{\partial\varepsilon}{\partial t} - \sigma_m + \frac{1}{a_w l}\rho T_1 \frac{\sigma_m}{T}\varepsilon_t \qquad (12)$$

The experimental data used in this research is obtained from ref. [29]. SMA material is typically commercially available $Ni_{50}Ti_{50}$ wire. The NiTi wire has a 0.76 mm diameter, total length $l = 60$ mm, and wire area of $a_w = 0.456$ mm^2. The density of the material is $\rho = 6.5\times10^6$ g/m^3, reference temperature $T_1 = 251$ K. The maximum value of. Differential Scanning Calorimetry (DSC) shows the various transition temperatures and latent heat values (Figure 2a). The stress–free phase at room temperature is austenite. The value of ε_t is estimated experimentally as 0.046 [33] for typical commercial SMA wire.
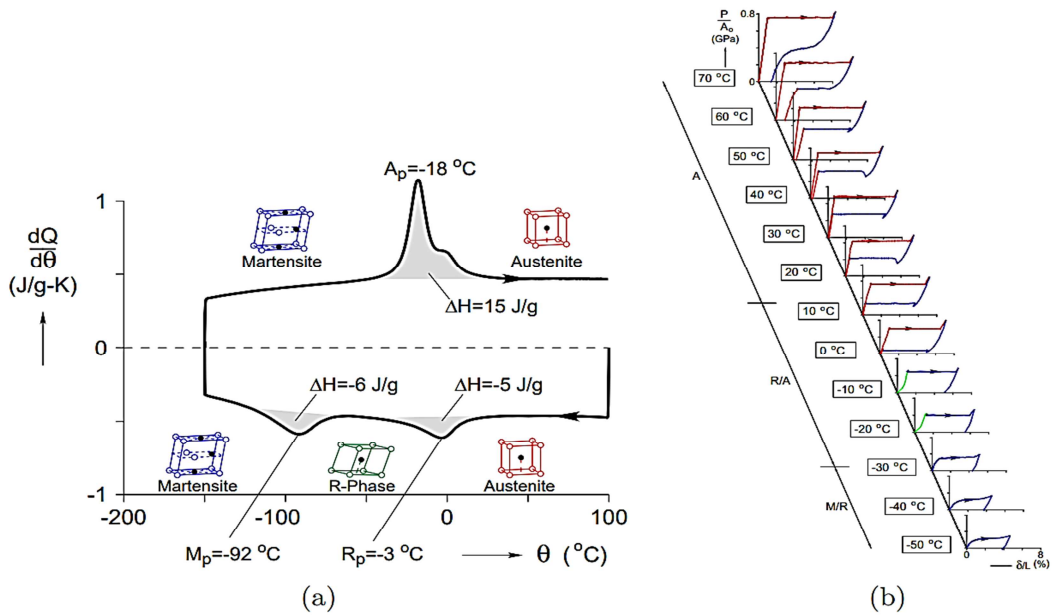

Figure 2. Experimental characterization of NiTi wire: (a) differential scanning calorimetry (DSC), (b) fundamental force-displacement responses [29].

The elastic term of stress is computed using Artificial Neutral Network (ANN), and its diagram is shown in Figure 3 with the stain as input and $e(\varepsilon, T)$ as output. The ANN has one hidden layer and three hidden units.
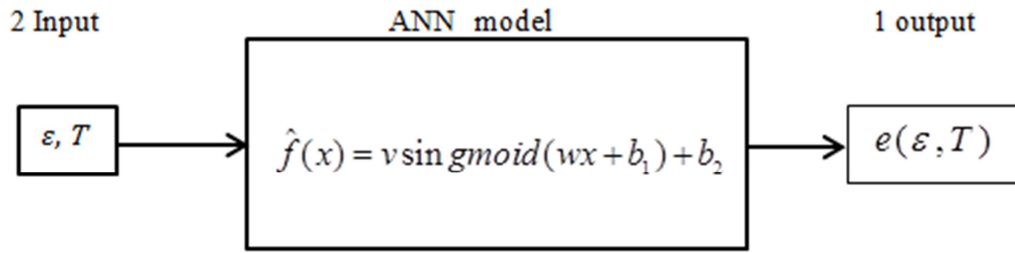
Figure 3. Structural diagram of ANN.

The ANN uses the following equation:

$$\hat{f}(x) = v \sin gmoid(wx + b_1) + b_2, \qquad (13)$$

where w and v are weight in the neutral network, b_1 and b_2 are biased in Neutral Network NN, w is a $n \times 1$ matrix, v is $1 \times n$ matrix, b_2 is 1×1 matrix, n is the number of the hidden units, which here are three, and the sigmoid (x).

Figure 4 shows the elastic term of stress as a function of strain. It is showed that when $e(\varepsilon, T)$ is generated, the effect of hysteresis by loading-unloading is almost eliminated.
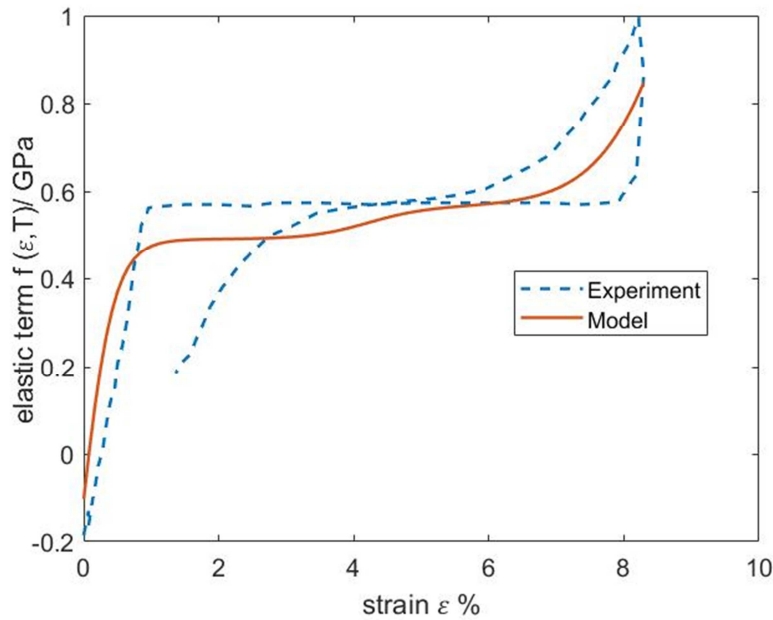

Figure 4. Stress versus strain graph.

3. Parameter Identification

The parameters of the proposed model are μ, w, v, b_1 and b_2. For ANN, there are 13 parameters. For a set of model parameters, given the stress, the strain is computed according to:

$$\mu \dot{\varepsilon} + v \sin gmoid(wx + b_1) + b_2 = \sigma. \qquad (14)$$

The least-square estimation method makes the simulated strains as close as possible to the experimental ones in the sense of least square error. This method transforms the parameter identification problem into a non-linear optimization problem. It is expressed as follows:

$$\min_{\mu, w, v, b_1 b_2} \frac{1}{n} \sum_{i=1}^{n} (\hat{\varepsilon}_i - \varepsilon_i)^2. \qquad (15)$$

4. Numerical Experiment

Using the above strategy, Figure 5(a) presents the comparison between the model and its experimental counterpart at the temperature of 343 K 70°C. The solid line shows the experimental result and the model by the dashed line. There is good agreement between the model and the experimental result, showing that the developed model has accurately simulated stress as a function of strain. Figure 5(b) shows the mean squared error changes during the optimization process. It shows both errors through rough and more precise methods, with a roughly estimated error at the beginning of the iteration. To get the energy function with respect to strain, the relationship gotten by ANN is numerically integrated. This is shown in Figure 5(c). The energy function has one local minima point.

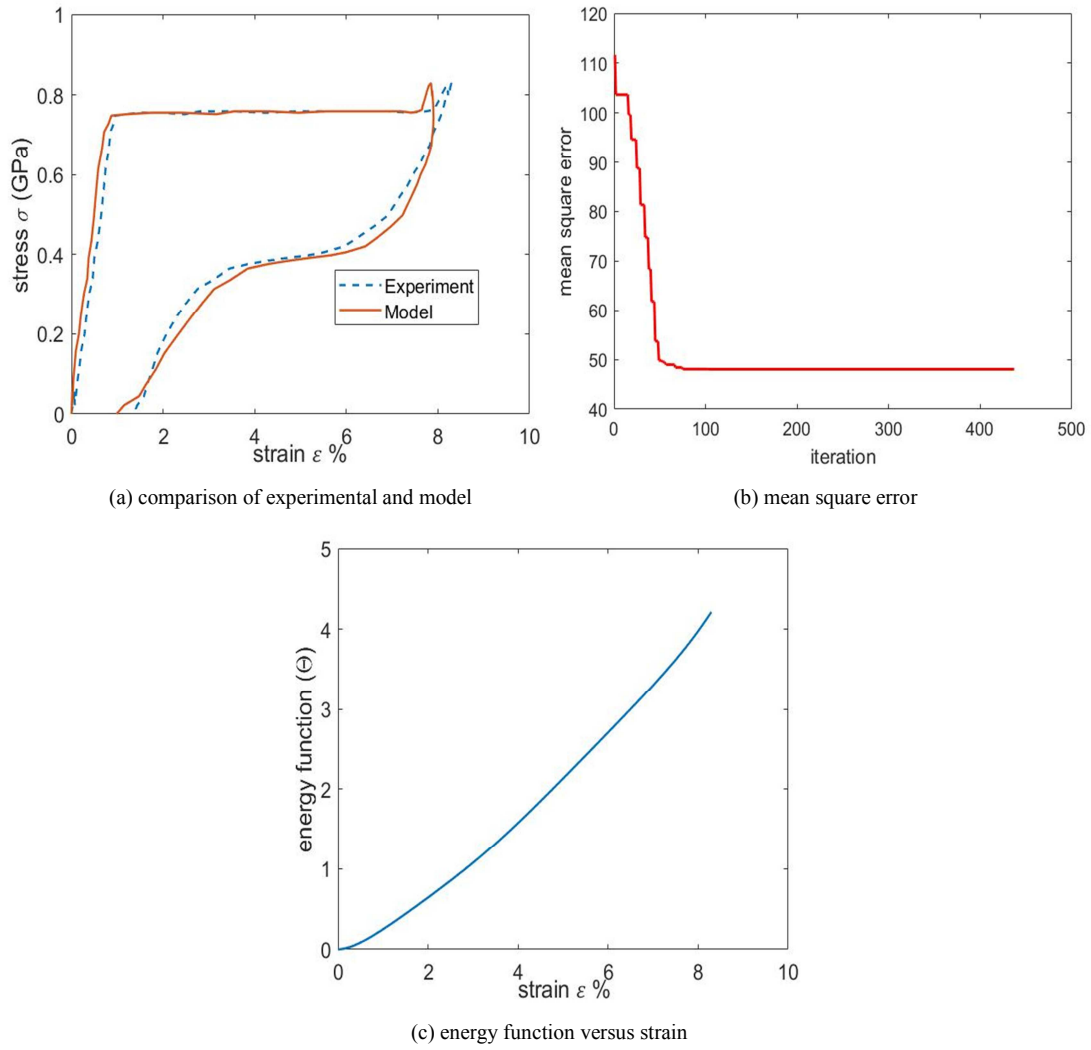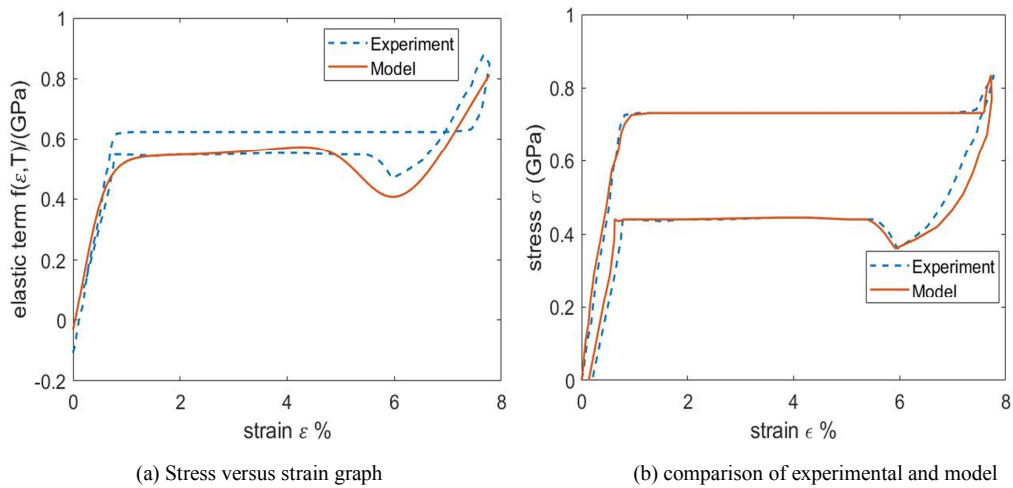The energy function is just a straight line with a minimum point at zero origin.

(a) comparison of experimental and model

(b) mean square error

(c) energy function versus strain

Figure 5. Simulation results for experimental data at 343 K (70°C).

The simulation is repeated using experimental data at 313 k (40°C) [32], and the results are presented in Figure 6. Figure 6(a) shows the elastic term of stress as a function of strain. It is showed that when $e(\varepsilon, T)$ is generated, the effect of hysteresis by loading-unloading is narrow. Figure 6(b) presents the comparison between the model and its experimental counterpart. The solid line shows the experimental result and the model by the dashed line. There is good agreement between the model and the experimental result, indicating that the proposed model can accurately simulate stress as a function of strain.
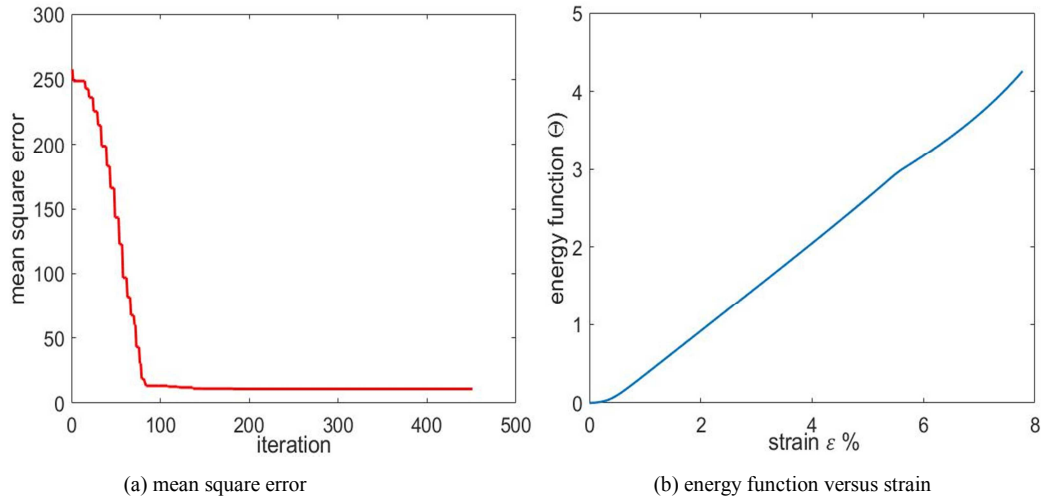

(a) Stress versus strain graph

(b) comparison of experimental and model

(a) mean square error

(b) energy function versus strain

Figure 6. Simulation results for experimental data at 313 K (40°C).

Figure 7 shows another commercial Ti–50.0 at.% Ni alloy [30] experimental data. It is used to further test the proposed model. The material has length $l = 100$, mass $m = 5$ mg,

diameter $d = 0.5$ mm, and the transition temperatures are $M_s = 337$ K, $M_f = 328$ K, $A_s = 355$ K, $A_f = 369$ K.
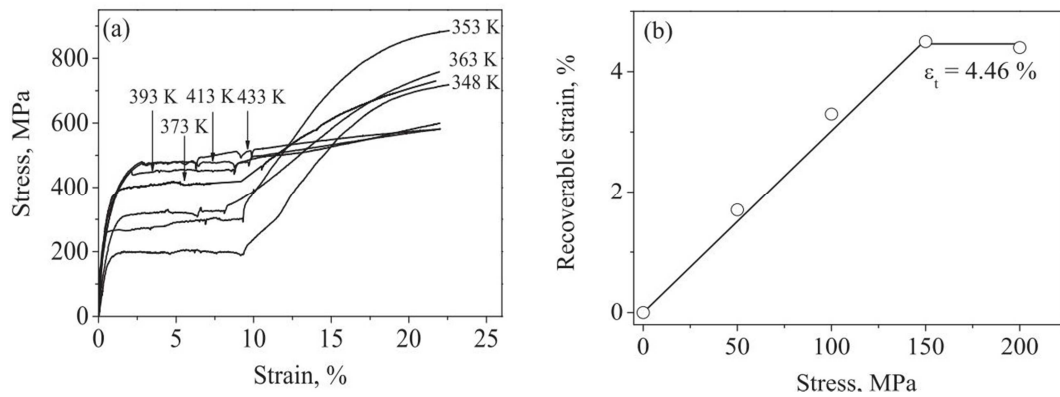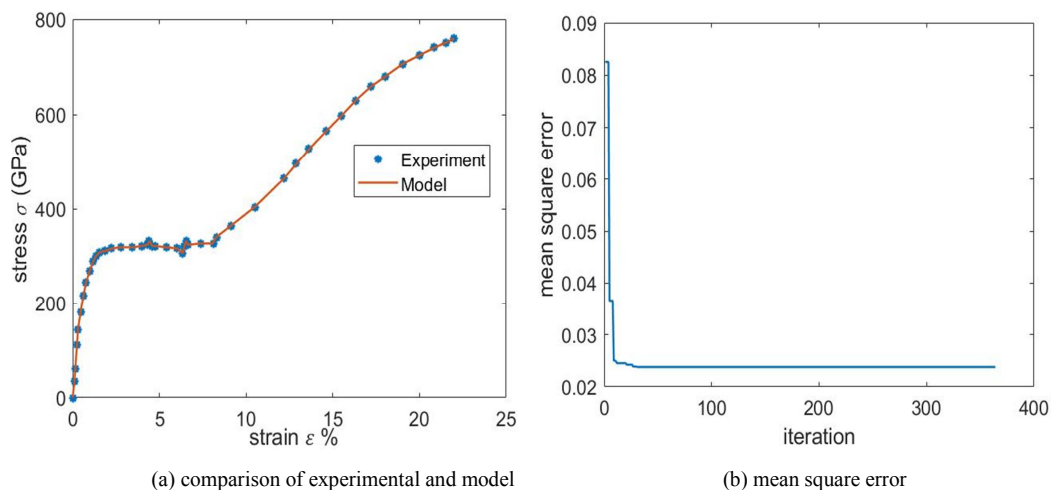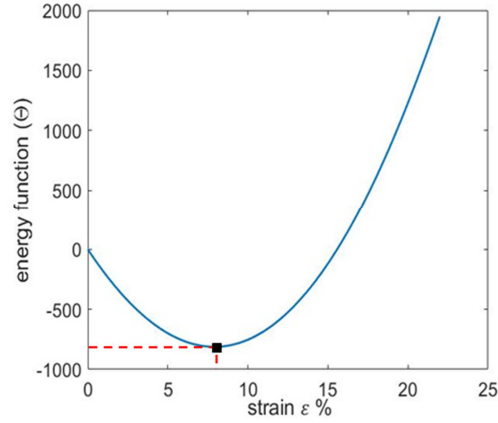

Figure 7. Experimental characterization of Ti–50.0 at.% Ni wire: (a) stress versus strain (b) recoverable strain versus stress for determining transformation strain (ε_t) [30].

Using the same strategy, Figure 8(a) presents the comparison between the model and its experimental counterpart. There is perfect agreement between the model and the experimental, indicating that the proposed model is accurate. The mean square error changes during the

optimization are shown in Figure 8(b). It shows both errors during the iteration. To get the energy function with respect to strain, the relationship gotten by ANN is numerically integrated. This is shown in Figure 8(c). The energy function has one local minima point.

(a) comparison of experimental and model

(b) mean square error

(c) energy function versus strain

Figure 8. *Simulation results for the second experimental data at 363 K.*

Figure 9(a) shows the comparison between the model and its experimental counterpart. There is perfect agreement between the model and the experimental, indicating that the proposed model is correct. Figure 9(b) shows the mean squared error changes during the optimization process. It shows both errors during the iteration. To get the energy function with respect to strain, the relationship gotten by ANN is numerically integrated. This is shown in Figure 9(c). The energy function has one local minima point.
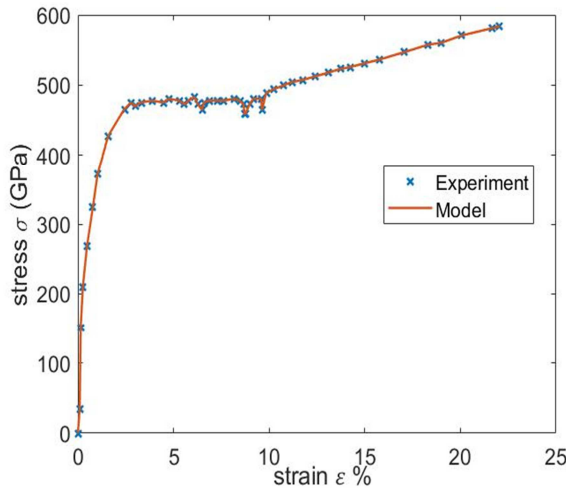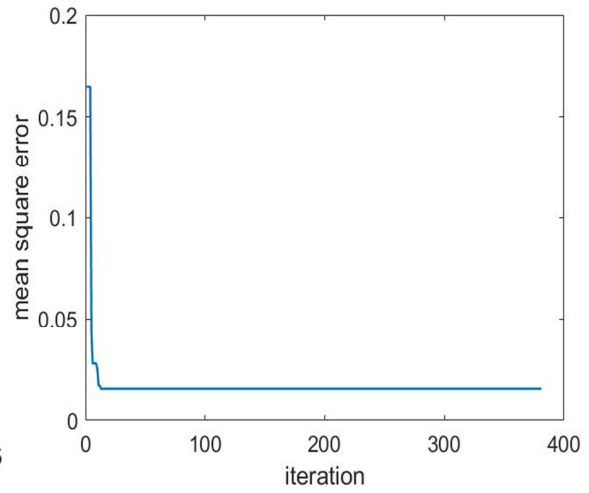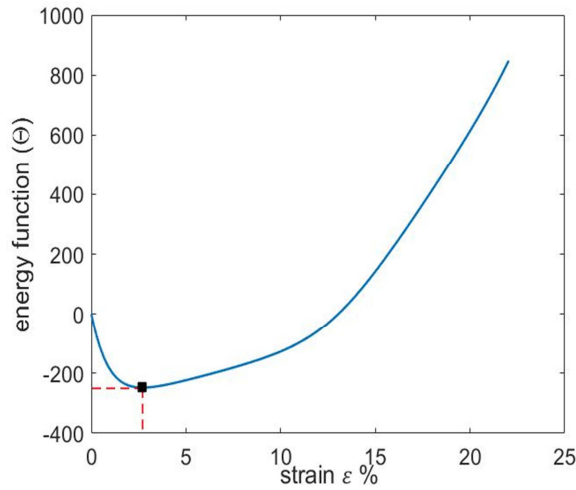

(a) comparison of experimental and model

(b) mean square error

(c) energy function versus strain

Figure 9. *Simulation results for the second experimental data at 413 K.*

5. Conclusion

In this paper, a one-dimensional phenomenological constitutive model of SMA material is proposed. Uniaxial tension and compression experimental of SMA is studied and constitutive relationship curved is obtained. In the proposed model the stress is divided into three parts: viscous, elastic, and chemical terms. Simulation of the elastic part is done using ANN, then the nonlinear optimization algorithm is used to optimize the parameters. The numerical experimental is carried out which captures well the constitutive relationship curved from uniaxial tension and compression experiments of SMA, thus the model can be verified.

Author contributions

Rabiu Ahmad Abubakar contributes to the conception, and performing design and simulation.

Conflicts of interest

The authors declare no conflicts of interest.

Data and Code Availability

The experimental data can be obtained in the references.

References

[1] P. Sittner, "Deformation twinning in martensite affecting functional behavior of NiTi shape memory alloys," *Materialia*, vol. 9, no. March, p. 100506, 2019.

[2] L. G. Machado, M. A. Savi, R. De Janeiro, and R. De Janeiro, "Medical applications of shape memory alloys," *Brazilian J. Med. Biol. Res.*, vol. 36, no. 6, pp. 683–691, 2003.

[3] M. R. Nagendra, M. Tamilselvan, and C. Sadhasivam, "Computation and investigation of an SMA engine using low heat recovery," *Int. J. Pure Appl. Math.*, vol. 118, no. 20, pp. 57–62, 2018.

[4] A. M. Halahla *et al.*, "The effect of shape memory alloys on the ductility of exterior reinforced concrete beam-column joints using the damage plasticity model," *Eng. Struct.*, vol. 200, no. September, p. 109676, 2019.

[5] S. Shiva, N. Yadaiah, I. A. Palani, C. P. Paul, and K. S. Bindra, "Thermo-mechanical analyses and characterizations of TiNiCu shape memory alloy structures developed by laser additive manufacturing," *J. Manuf. Process.*, vol. 48, no. February 2018, pp. 98–109, 2019.

[6] J. J. Zhu, N. G. Liang, W. M. Huang, and K. M. Liew, "Energy conversion in shape memory alloy heat engine part I: Simulation," *J. Intell. Mater. Syst. Struct.*, vol. 12, no. 2, pp. 133–140, 2001.

[7] V. N. Melnik Roderick, L. Wang, P. Matus, and I. Rybak, "Computational aspects of conservative difference schemes for shape memory alloys," in *International Conference on Computational Science and Its Applications*, C. L. Gerhard Goos, Juris Hartmanis, Ed., Berlin, Heidelberg: Springer, 2003, pp. 791–800.

[8] L. Wang and R. V. N. Melnik, "Thermo-mechanical wave propagations in shape memory alloy rod with phase transformations," *Mech. Adv. Mater. Struct.*, vol. 14, no. 8, pp. 665–676, 2007.

[9] C. B. Churchill and J. Shaw, "Thermo-mechanical modeling of shape memory allow heat engine," in *Proceedings of the ASME 2011 Conference on Smart Materials, Adaptive Structures and Intelligent Systems*, Scottsdale, Arizona, USA: ASME, 2011, pp. 641–650.

[10] L. LECCE and C. Antonio, *Shape Memory Alloy Engineering*. Amsterdam: Elsevier, 2015.

[11] V. Alexandrakis, J. Manuel, and A. Pérez-checa, "Combinatorial synthesis of Ni–Mn–Ga-(Fe, Co, Cu) high temperature ferromagnetic shape memory alloys thin films," *Scr. Mater.*, vol. 178, no. March, pp. 104–107, 2020.

[12] E. Fritsch, M. Izadi, and E. Ghafoori, "Development of nail-anchor strengthening system with iron-based shape memory alloy (Fe-SMA) strips," *Constr. Build. Mater.*, vol. 229, p. 117042, 2019.

[13] H. Huang, P. Yao, and Y. Su, "Stress relaxation behavior of columnar-grained Cu-Al-Mn shape memory alloys," *Mater. Sci. Eng. A*, vol. 768, no. September, p. 138432, 2019.

[14] X. Fei, Y. Haifeng, L. Kun, M. Jiaxiang, and C. Haoxue, "Forming and two-way shape memory effect of NiTi alloy induced by laser shock imprinting," *Opt. Laser Technol.*, vol. 120, no. April, p. 105762, 2019.

[15] P. Honarmandi, L. Johnson, and R. Arroyave, "Bayesian probabilistic prediction of precipitation behavior in Ni-Ti shape memory alloys," *Comput. Mater. Sci.*, vol. 172, no. September 2019, 2020.

[16] D. Patil and G. Song, "Shape memory alloy actuated accumulator for ultra-deepwater oil and gas exploration," *Smart Mater. Struct.*, vol. 25, no. 4, 2016, doi: 10.1088/0964-1726/25/4/045012.

[17] L. Pellone, S. Ameduri, N. Favaloro, and A. Concilio, "SMA-based system for environmental sensors released from an unmanned aerial vehicle," *Aerospace*, vol. 4, no. 1, 2017, doi: 10.3390/aerospace4010004.

[18] G. Costanza, G. Leoncini, F. Quadrini, and M. E. Tata, "Design and Characterization of a Small-Scale Solar Sail Prototype by Integrating NiTi SMA and Carbon Fibre Composite," in *Advances in Materials Science and Engineering*, D. C. Lagoudas, Ed., TX. USA: 8 Springer Science+Business Media, LLC, 2017, p. 1. doi: 10.1155/2017/8467971.

[19] U. Roshan, J. B. Basnayake, R. Amarasinghe, and N. Dayananda, "Design and Development of a Force Feedback System for a SMA Based Gripper as a Minimally Invasive Surgical Tool," *Proc. IEEE Sensors*, vol. 2019-Octob, no. July 2021, pp. 1–4, 2019, doi: 10.1109/SENSORS43011.2019.8956849.

[20] S. H. Adarsh and V. Sampath, "Hot deformation behavior of Fe-28Ni-17Co-11.5Al-2.5Ta-0.05B (at.%) shape memory alloy by isothermal compression," *Intermetallics*, vol. 115, no. December, p. 106632, 2019.

[21] H. Cho, Y. Takeda, and T. Sakuma, "Fabrication and output power characteristics of heat-engines using tape-shaped SMA element," *Adv. Struct. Mater.*, vol. 73, pp. 1–15, 2017.

[22] A. Paiva and M. A. Savi, "An overview of constitutive models for shape memory alloys," *Math. Probl. Eng.*, vol. 2006, no. September 2004, pp. 1–30, 2006, doi: 10.1155/MPE/2006/56876.

[23] F. Auricchio and E. Sacco, "A one-dimensional model for superelastic shape-memory alloys with different elastic properties between austenite and martensite," *Int. J. Non. Linear. Mech.*, vol. 32, no. 6, pp. 1101–1114, 1997, doi: 10.1016/s0020-7462(96)00130-8.

[24] R. Abeyaratne and J. K. Knowles, "A continuum model of a thermoelastic solid capable of undergoing phase transitions," *J. Mech. Phys. Solids*, vol. 41, no. 3, pp. 541–571, 1993, doi: 10.1016/0022-5096(93)90048-K.

[25] T. Kikuak, K. Shigenori, and S. Yoshio, "Thermomechanics of transformation pseudoelasticity and shape memory effect in alloys," *Int. J. Plast.*, vol. 2, no. 1, pp. 59–72, 1986.

[26] C. A. Liang, C., & Rogers, "One-dimensional thermo-mechanical constitutive relations for shape memory materials," *J. Intell. Mater. Syst. Struct.*, vol. 1(2), pp. 207-234., 1990.

[27] L. C. Brinson, "One-dimensional constitutive behavior of shape memory alloys: Thermomechanical derivation with non-constant material functions and redefined martensite internal variable," *J. Intell. Mater. Syst. Struct.*, vol. 4, no. 2, pp. 229–242, 1993.

[28] F. Wang and L. Wang, "A phenomenological constitutive model for one-dimensional shape memory alloys based on artificial neural network," vol. 32, no. 1983, pp. 2338–2348, 2021, doi: 10.1177/1045389X21995876.

[29] B. C. Chang, J. A. Shaw, and M. A. Iadicola, "Thermodynamics of shape memory alloy wire: Modeling, experiments, and application," *Contin. Mech. Thermodyn.*, vol. 18, no. 1–2, pp. 83–118, 2006, doi: 10.1007/s00161-006-0022-9.

[30] R. Natalia and B. Sergey, "Entropy change in the B2 → B19′ martensitic transformation in TiNi alloy," *Thermochim. Acta*, vol. 602, pp. 30–35, 2015, doi: 10.1016/j.tca.2015.01.004.